The Canadian Mineralogist
Vol. 34, pp. 881-892 (1996)

PHASE TRANSITIONS IN THE SERIES BORACITE – TREMBATHITE – CONGOLITE: PHASE RELATIONS

PETER C. BURNS[1] AND MICHAEL A. CARPENTER

Department of Earth Sciences, University of Cambridge, Downing Street, Cambridge CB2 3EQ, U.K.

ABSTRACT

The Sussex, New Brunswick, marine-evaporite-hosted borate deposits contain boracite-group minerals of the solid-solution series $Mg_3B_7O_{13}Cl$ – $Fe_3B_7O_{13}Cl$. Samples of boracite, trembathite and congolite have been characterized by electron-probe microanalysis and by high-temperature optical examination and X-ray powder diffraction. At 25°C, the orthorhombic boracite structure ($Pca2_1$) is stable for compositions from $Mg_3B_7O_{13}Cl$ to $(Mg_{1.9}Fe_{1.1})B_7O_{13}Cl$, and the rhombohedral congolite structure ($R3c$) occurs for compositions ranging from $(Mg_{1.9}Fe_{1.1})B_7O_{13}Cl$ to $Fe_3B_7O_{13}Cl$. At high temperatures, all specimens examined have the cubic boracite structure ($F\bar{4}3c$). Cooling results in a first-order phase transition to the orthorhombic structure, and specimens with more than 36 mol.% $Fe_3B_7O_{13}Cl$ undergo a further first-order phase transition to the rhombohedral structure. The boundaries between the phases with cubic, orthorhombic and rhombohedral structures are linear in composition-temperature space. There is a marked discontinuity in the unit-cell volume of specimens rich in Mg at the phase transition from the cubic to the orthorhombic structure; the positive volume strain is greatest in the Mg-rich samples. The high-temperature X-ray diffraction data show that the cubic-to-orthorhombic phase transition is first order in samples rich in Mg, but increasing Fe content results in a trend toward tricritical or second-order character. Higher Fe contents are associated with a decrease in the absolute value of the volume strain due to the phase transition. Although the symmetry-breaking strain due to the phase transition is very small, it is revealed by the variation in peak width as a function of temperature in the X-ray powder diffractograms.

Keywords: boracite, trembathite, congolite, phase transition, phase relations, solid solution, mineral physics.

SOMMAIRE

Les dépôts de borate de Sussex, au Nouveau-Brunswick, d'origine évaporitique marine, contiennent des minéraux du groupe de la boracite, membres de la solution solide $Mg_3B_7O_{13}Cl$ – $Fe_3B_7O_{13}Cl$. Nous avons caractérisé les échantillons de boracite, trembathite et congolite par analyse à la microsonde électronique, par examen des propriétés optiques à température élevée, et par diffraction X. A 25°C, la structure de la boracite orthorhombique ($Pca2_1$) s'applique aux compositions dans l'intervalle $Mg_3B_7O_{13}Cl$ à $(Mg_{1.9}Fe_{1.1})B_7O_{13}Cl$, et la structure rhomboédrique de la congolite ($R3c$) s'applique aux compositions dans l'intervalle entre $(Mg_{1.9}Fe_{1.1})B_7O_{13}Cl$ à $Fe_3B_7O_{13}Cl$. A température élevée, tous les spécimens étudiés possèdent la structure de la boracite cubique ($F\bar{4}3c$). Un refroidissement cause une inversion de premier ordre à la structure orthorhombique; de plus, tout échantillon contenant plus de 36% de $Fe_3B_7O_{13}Cl$ (base molaire) subit une deuxième transition, à la structure rhomboédrique. Les limites des champs de stabilité des phases ayant les structures cubique, orthorhombique et rhomboédrique sont linéaires dans un diagramme de composition *versus* température. Nous décelons une discontinuité importante dans le volume de la maille élémentaire dans le cas d'échantillons riches en Mg en passant de la structure cubique à la structure orthorhombique; la distorsion du réseau associée à la transition est plus importante dans les échantillons les plus riches en Mg. Les données de diffraction X obtenues à température élevée montrent que cette transition a un caractère de premier ordre dans le cas d'échantillons riches en Mg, mais avec une augmentation en Fe, son caractère devient tricritique ou de deuxième ordre. Les teneurs plus élevées en Fe mènent à une diminution du degré de distorsion volumique due à l'inversion. La distorsion associée à l'inversion requise pour réduire la symétrie est très faible; malgré ceci, la largeur des pics de diffraction en fonction de la température en est un reflet sensible.

(Traduit par la Rédaction)

Mots-clés: boracite, trembathite, congolite, transition de phase, relations de phases, solution solide, physique minérale.

---

[1] *Present address:* Department of Geology, University of Illinois at Urbana-Champaign, 245 Natural History Building, 1301 West Green Street, Urbana, Illinois 61801, U.S.A.

INTRODUCTION

Boracite-type phases have the general formula $M_3B_7O_{13}X$, where M is a divalent cation (Mg, Cr, Mn, Fe, Co, Ni, Cu, Zn, Cd), and X is a halogen atom (Cl, Br, I). These phases have been synthetically prepared and extensively studied, owing to the ferroelastic, ferroelectric and magnetic properties of the crystals (Nelmes 1974). Five of the boracite-type phases have been described as minerals (Table 1); all have Cl as the halogen, and four contain Mg and Fe as the divalent cation. Crystals of natural boracite-group minerals usually contain complex twinning and display anomalous optical properties, although some well-formed specimens show excellent large domains. Schmid & Tippmann (1978) provided an interesting historical overview of early studies of boracite-group minerals.

The phase transitions in boracite-type phases have received a great deal of attention over the past three decades because of possible applications in the material sciences. For example, boracite-type phases have been considered as possible components for optical page composers, optical storage, and passive display devices because they are ferroelectrics that permit optical contrast upon switching (Schmid & Tippmann 1978). A necessary requirement for using boracite-type phases in this context is the development of a composition having a very small shear angle in order to prevent cracking and various other detrimental effects outlined by Schmid & Tippmann (1978).

This study concerns phase relations in the series $Mg_3B_7O_{13}Cl$ – $Fe_3B_7O_{13}Cl$. The series includes the minerals boracite [$Mg_3B_7O_{13}Cl$], trembathite [$(Mg,Fe)_3B_7O_{13}Cl$] and congolite [$(Fe,Mg)_3B_7O_{13}Cl$]. The structure of boracite is orthorhombic at room temperature, whereas the structure of congolite is rhombohedral. Thus a solid-solution series between $Mg_3B_7O_{13}Cl$ and $Fe_3B_7O_{13}Cl$ must involve a phase transition. The purpose of this work is to characterize the phase relations in this system, both as a function of Mg:Fe ratio and of temperature. In later contributions, we will examine the microstructure in natural specimens (due to these phase transitions), and will illustrate how the microstructure relates to the thermal history of borate deposits.

Most of the boracite-group mineral specimens examined in this study are from the Penobsquis evaporite deposit, located in Sussex, New Brunswick. Since their discovery two decades ago, the marine-evaporite-hosted borate deposits at Sussex have received considerable attention (Roulston & Waugh 1981, Rachlin *et al.* 1986, Mandarino *et al.* 1990, Burns *et al.* 1992, Roberts *et al.* 1993, Grice *et al.* 1994). The Mississippian-age deposits occur in the Windsor Group of the Moncton sub-basin, a part of the northeasterly trending Fundy basin. Borate minerals are primarily located in the Upper Halite Member [nomenclature of Roulston & Waugh (1983); this is referred to as the Middle Halite Member by Roulston & Waugh (1981)]. Details of the geology of the evaporite deposits may be found in Roulston & Waugh (1983). In addition to a suite of a dozen or more previously recognized borate mineral species, mineralogical studies of these deposits have led to the descriptions of the boracite-group mineral trembathite (Burns *et al.* 1992) and the $Ca_9B_{26}O_{34}(OH)_{24}Cl_4{\cdot}13H_2O$ polymorphs pringleite and ruitenbergite (Roberts *et al.* 1993), whose structures bear similarities to those of aluminosilicate zeolites (Grice *et al.* 1994).

The Zechstein salt deposits of Germany also contain boracite-group minerals of a range of compositions. Heide & Völksch (1979) and Heide *et al.* (1980) have examined the borates in these deposits; their studies included chemical analyses, studies of crystal morphology by scanning electron microscopy, X-ray diffraction, and differential thermal analyses. The Zechstein deposits contain both well-formed pseudocubic crystals and fibrous intergrowths of boracite-group minerals. Heide & Völksch (1979) indicated that the pseudocubic crystals may have formed at several different times, and that intergrowths of mimetic twins are absent. This absence of twins indicates that the crystals grew in the stability field of the orthorhombic or rhombohedral structure, and that a phase transition has not occurred. Heide *et al.* (1980) reported chemical compositions for 21 specimens of boracite-group minerals from the Zechstein deposits. Crystal compositions range from end-member $Mg_3B_7O_{13}Cl$ to $(Fe_{2.54}Mn_{0.24}Mg_{0.22})B_7O_{13}Cl$.

TABLE 1. CELL DIMENSIONS OF BORACITE-GROUP MINERALS

		Space Group	a (Å)	b (Å)	c (Å)	Ref.
boracite	$Mg_3B_7O_{13}Cl$	$Pca2_1$	8.577(6)	8.553(8)	12.09(1)	1
ericaite	$(Fe,Mg)_3B_7O_{13}Cl$	$Pca2_1$	8.58	8.65	12.17	2
trembathite	$(Mg,Fe)_3B_7O_{13}Cl$	$R3c$	8.574(2)		20.99(1)	3
congolite	$(Fe,Mg)_3B_7O_{13}Cl$	$R3c$	8.622(1)		21.054(5)	4
chambersite	$Mn_3B_7O_{13}Cl$	$Pca2_1$	8.68(1)	8.68(1)	12.26(1)	5

References: (1) Burns (1995); (2) Kühn & Schaacke (1955); (3) Burns *et al.* (1992); (4) Wendling *et al.* (1972); (5) Honea & Beck (1962).

STRUCTURE AND PHASE TRANSITIONS

The crystal structures of all boracite-type phases have cubic symmetry, space group $F\bar{4}3c$, at high temperature. The structure of cubic boracite (Ito *et al.* 1951, Sueno *et al.* 1973) consists of a framework of corner-sharing BO_4 tetrahedra, with the metal and halogen atoms located within cavities in the borate framework (Fig. 1). Using the descriptor of Burns *et al.*

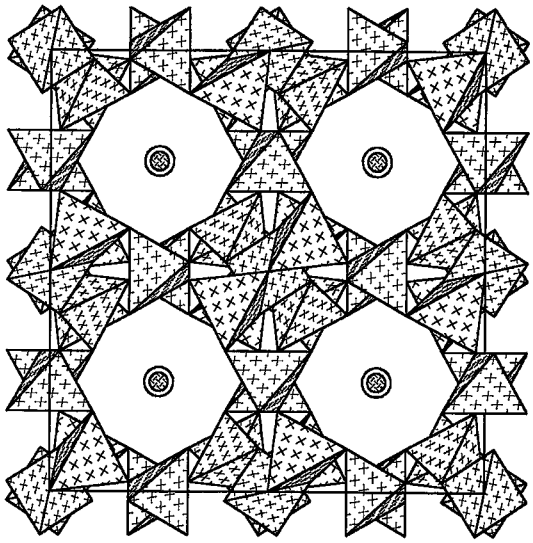

FIG. 1. The cubic boracite structure (Sueno *et al.* 1973) projected down [001]. BO_4 tetrahedra are shaded with crosses, Mg atoms as shown as circles shaded with a herring-bone pattern, and Cl atoms are shown as open circles. The cubic unit-cell is outlined.

(1995), the fundamental building block (FBB) for this structure is 4□:[ϕ]□|□|□|□|, indicating that a central oxygen atom is connected to four BO_4 tetrahedra. The structure of cubic boracite is the only structure known to contain an oxygen atom [O(1) using the notation of Sueno *et al.* 1973] that is bonded to four boron atoms. The O(1) atom is located on a site with point symmetry 23, and in cubic boracite, each of the four B(3)–O(1) bond-lengths is 1.693(5) Å (Sueno *et al.* 1973), a value considerably longer than $<^{[4]}B–O>$ = 1.476 Å found in minerals. The one metal site is coordinated by six ligands; four equidistant equatorial oxygen atoms and two equidistant halogen atoms are in a *trans* arrangement.

In most boracite-type phases (but not all), cooling of the cubic structure results in a phase transition, or a series of phase transitions, to a structure with lower symmetry. In the low-temperature structures, the O(1) position is bonded to three boron atoms only, and the borate framework contains both BO_4 tetrahedra and BO_3 triangles. At room temperature, the structure of boracite is orthorhombic, space group $Pca2_1$ (Dowty & Clark 1973), whereas the structures of trembathite and congolite have rhombohedral symmetry, space group *R*3*c* (Schmid 1970, Mendoza-Alvarez *et al.* 1985, Burns *et al.* 1992). Using the descriptor of Burns *et al.* (1995), the borate FBB of both the $Pca2_1$ and *R*3*c* structures is Δ6□:[ϕ]<3□>|<3□>|<3□>|Δ. The $Pca2_1$ and *R*3*c* structures contain three and one symmetry-distinct metal sites, respectively. In each case, the coordination geometry of the cation is significantly distorted from the arrangement of the cubic structure.

The phase transition from the cubic boracite structure, space group $F\bar{4}3c$, to the orthorhombic structure, space group $Pca2_1$, is an improper ferroelastic phase-transition (Dvořák & Petzelt 1971) that involves a doubling of the volume of the primitive unit-cell (Ito *et al.* 1951). The orthorhombic and rhombohedral unit-cells are obtained from the cubic unit-cell *via* the transformation matrices [½, ½, 0, –½, ½, 0, 0, 0, 1] and [½, 0, ½, – ½, ½, 0, –1, –1, 1], respectively.

Upon heating, synthetic $Mg_3B_7O_{13}Cl$ undergoes a single phase-transition from the orthorhombic structure ($Pca2_1$) to the cubic structure ($F\bar{4}3c$) at ~264°C (Schmid & Tippmann 1978). When heated, synthetic $Fe_3B_7O_{13}Cl$ undergoes a series of first-order phase-transitions from the rhombohedral structure (*R*3*c*), first to a monoclinic structure (*Pc*) at ~255°C, then to an orthorhombic structure ($Pca2_1$) at ~270°C, and finally to a cubic structure ($F\bar{4}3c$) at ~336°C (Schmid & Tippmann 1978).

EXPERIMENTAL

Sample description

The specimens studied, all but one from the Potash Company of Saskatchewan mine workings, are currently housed at the Canadian Museum of Nature (CMN) in Ottawa, Ontario. Each sample suite contains one or more sections of diamond-drill core from the Upper Halite Member. In addition to halite, each drill core contains an assemblage of borate minerals, which includes hilgardite, hydroboracite, and the boracite-group minerals. Pieces of drill core were dissolved in warm water, and boracite-group minerals were selected from the insoluble portion. Samples S4A and S4B are from CMN suite F93–20–4, which contains one section of drill core. Samples S8A to S8E are from CMN suite F93–20–8, which contains three sections of drill core. In addition, one specimen of near-end-member boracite from England (EB, locality unknown) was studied.

Single pseudocubic crystals of boracite-group minerals ranging up to 3 mm in diameter were selected for study. These crystals show prominent $(001)_{cubic}$ growth faces, and less prominent $(111)_{cubic}$ growth faces. Each crystal was cut in half parallel to $(001)_{cubic}$ using a microsaw. Half was used to prepare a doubly-polished section for optical examination and subsequent chemical analysis using the electron microprobe. The other half was set aside for examination using a transmission electron microscope (results to be reported in a subsequent paper).

TABLE 2. ELECTRON-MICROPROBE DATA FOR BORACITE-GROUP MINERALS*

	S8-A	S8-B	S8-C	S8-D	S8-E	S4-A	S4-B	EB
# Points	15	24	28	28	30	6	30	35
FeO	25.54(35)	26.33(55)	23.89(56)	37.01(1.59)	36.30(1.24)	12.57(42)	12.40(29)	3.24(34)
MnO	0.26(4)	0.24(4)	0.38(5)	1.00(12)	0.84(12)	0.89(7)	0.90(5)	0.03(3)
MgO	13.52(40)	13.10(43)	14.95(35)	4.45(1.25)	5.02(95)	22.35(34)	22.16(46)	30.52(48)
Cl	7.83(13)	7.62(13)	8.08(9)	7.49(8)	7.48(8)	8.30(10)	8.47(6)	8.25(40)
B_2O_3	56.42	56.43	57.57	51.94	52.11	60.26	59.71	65.21
Cl=O	-1.77	-1.72	-1.82	-1.69	-1.69	-1.87	-1.91	-1.86
Total	101.80	102.01	103.06	100.19	100.06	102.50	101.73	105.39
Fe^{2+}	1.55(3)	1.58(4)	1.41(3)	2.42(13)	2.36(10)	0.71(1)	0.70(2)	0.17(2)
Mn^{2+}	0.00(2)	0.015(3)	0.023(3)	0.07(1)	0.06(1)	0.050(3)	0.052(3)	0.002(2)
Mg	1.45(3)	1.40(4)	1.57(3)	0.52(14)	0.58(11)	2.24(1)	2.24(2)	2.83(2)
Cl	0.95(2)	0.93(2)	0.96(1)	0.99(1)	0.99(1)	0.95(1)	0.97(1)	0.87(5)

* B_2O_3 calculated from stoichiometry; formula calculation assumes Fe + Mn + Mg = 3

Electron-microprobe analysis

Single crystals were cut, mounted in epoxy, polished, and coated with carbon for electron-microprobe analysis. Compositions were determined using a Cameca SX50 probe operated in wavelength-dispersion mode. The acceleration voltage was 20 kV, and the beam current was 15 nA; the samples were found to be stable under these conditions. The following standards were used: MgO (Mg), Fe metal (Fe), NaCl (Cl), Mn metal (Mn) and wollastonite (Ca). Multiple points were analyzed for each sample; average values for each sample, along with the corresponding standard deviation, are reported in Table 2. The concentration of boron was calculated from stoichiometry.

Significant Fe – Mg zonation is apparent in back-scattered images, and in the relatively high standard deviations of the average analysis for each specimen (Table 2). The large $(001)_{cubic}$ growth-sectors contain concentric zones parallel to the growth faces that become progressively more iron-rich moving from the core to the rim. In addition, $(111)_{cubic}$ growth-sectors are in some cases present, and are enriched in either Mg or Fe relative to the adjacent $(001)_{cubic}$ growth-sectors. These sector zones also contain concentric zoning parallel to the $(111)_{cubic}$ growth-face. Some crystals contain a prominent Fe-rich overgrowth. Compositions from small $(111)_{cubic}$ sector-zones and overgrowths were excluded from the averages reported in Table 2.

Room-temperature X-ray powder diffraction

Samples for X-ray powder-diffraction experiments were crushed and ground in an agate mortar for several minutes. Silicon was added as an internal standard, and smear mounts were prepared on low-background lead-glass. Diffraction patterns were collected at 25°C with an automated Siefert X-ray powder diffractometer with Bragg–Brentano geometry using Cu$K\alpha$ X-radiation (20 mA, 30 kV), a fixed 1-mm divergence slit, a 1° receiving slit, and a diffracted-beam monochromator. Preliminary scans showed the patterns to be featureless below 14°2θ; data were collected over the range 14 – 100°2θ with a step interval of 0.02°2θ and a count time of 60 s per step. The symmetry of each sample (Table 3) was determined by comparison of the powder patterns to those given by Burns (1995).

High-temperature X-ray powder diffraction

Samples for high-temperature X-ray powder-diffraction experiments were ground in an agate mortar for several minutes. Silicon was added as an internal standard. The samples were smeared onto a heating device that consisted of a platinum strip pulled mechanically onto a ceramic plate. The sample thickness was roughly 0.2 mm, and the temperature was monitored using a platinum – 13% rhodium thermocouple welded to the underside of the platinum strip. The temperature was calibrated against the transition points of various standards mounted in the same configuration; the uncertainty of the temperature scale is ±10°C. Diffraction data were collected

TABLE 3. ROOM-TEMPERATURE SYMMETRY AND PHASE-TRANSITION TEMPERATURES FOR BORACITE-GROUP MINERALS

	Mineral Name	M Formula	Room T. Structure	$R3c \leftrightarrow Pca2_1$	$Pca2_1 \leftrightarrow F\bar{4}3c$
S8-A	congolite	$Fe_{1.55}Mg_{1.45}$	*R3c*	87 ± 12°C	311 ± 5°C
S8-B	congolite	$Fe_{1.58}Mg_{1.40}Mn_{1.01}$	*R3c*	95 ± 10	307 ± 6
S8-C	trembathite	$Mg_{1.57}Fe_{1.41}Mn_{0.02}$	*R3c*	60 ± 17	303 ± 5
S8-D	congolite	$Fe_{2.42}Mg_{0.52}Mn_{0.07}$	*R3c*	217 ± 7	320 ± 2
S8-E	congolite	$Fe_{2.36}Mg_{0.58}Mn_{0.06}$	*R3c*	208 ± 7	319 ± 3
S4-A	boracite	$Mg_{2.24}Fe_{0.71}Mn_{0.05}$	*Pca2₁*		287 ± 3
S4-B	boracite	$Mg_{2.24}Fe_{0.70}Mn_{0.06}$	*Pca2₁*		283 ± 2
EB	boracite	$Mg_{2.83}Fe_{0.17}$	*Pca2₁*		272 ± 5
		Fe_3*			336
		Mg_3*			264

*from Schmid & Tippmann (1978)

TABLE 4. HIGH-TEMPERATURE UNIT-CELL PARAMETERS AND UNIT-CELL VOLUME FOR EB

T (°C)	a (Å)	V (Å³)	T (°C)	a (Å)	V (Å³)
20	12.0937(5)	1768.8(2)	257	12.1057(5)	1774.1(2)
20*	12.0942(5)	1769.0(2)	261	12.1039(6)	1773.3(2)
97	12.0991(6)	1771.2(3)	266	12.1039(4)	1773.3(2)
121	12.1026(5)	1772.7(2)	290	12.1056(5)	1774.0(2)
146	12.1041(5)	1773.3(2)	314	12.1067(6)	1774.5(3)
170	12.1055(5)	1774.0(2)	339	12.1094(5)	1775.7(2)
194	12.1063(5)	1774.3(2)	363	12.1114(5)	1776.6(2)
218	12.1073(5)	1774.7(2)	387	12.1128(5)	1777.2(2)
242	12.1082(5)	1775.1(2)	411	12.1148(7)	1778.1(3)
242*	12.1075(5)	1774.9(2)	435	12.1163(5)	1778.7(2)
247	12.1076(5)	1774.9(2)	459	12.1188(4)	1779.8(2)
252	12.1072(5)	1774.7(2)	483	12.1205(6)	1780.6(3)

* obtained after cooling

using monochromated Cu$K\alpha_1$ X-radiation (22 mA, 35 kV) and a 4K–PSD INEL detector (as described by Salje *et al.* 1993). The diffraction signals were measured between $2\theta_{min} = 8$ and $2\theta_{max} = 120°$ for 3 hours per temperature setting, and data were corrected using all ten reflections corresponding to the silicon internal standard. Unit-cell parameters (Tables 4, 5, 6) were refined using the least-squares program of Appleman & Evans (1973). The least-squares refinements for samples with cubic symmetry included ~35 reflections, whereas those for samples with rhombohedral and orthorhombic symmetry included ~55 reflections. The unit cells of the rhombohedral and orthorhombic structures are dimensionally cubic within the resolution of conventional X-ray powder diffraction (Burns 1995). Hence, all unit-cell refinements were performed using cubic unit-cell constraints, and the reported dimensions are given in the cubic setting.

Owing to the lack of a diffracted-beam monochromating device, and the fluorescence of Fe in Cu X-radiation, background counts increased dramatically with increasing Fe content of the samples. Owing to a poor peak-to-background ratio, the precision of the determined unit-cell parameters decreases significantly with increasing Fe, to the extent that useful data could not be obtained for the most Fe-rich specimens. Therefore, data are reported for samples EB, S4–A and S8–A only.

TABLE 5. HIGH-TEMPERATURE UNIT-CELL PARAMETERS AND UNIT-CELL VOLUME FOR S4-A

T (°C)	a (Å)	V (Å³)	T (°C)	a (Å)	V (Å³)
20	12.1173(6)	1779.1(3)	223	12.1271(8)	1783.5(3)
20*	12.1169(5)	1779.0(2)	232	12.1271(7)	1783.5(3)
39	12.1204(6)	1780.5(3)	242	12.1275(6)	1783.7(3)
59	12.1208(6)	1780.7(3)	252	12.1276(6)	1783.7(3)
78	12.1220(6)	1781.2(3)	261	12.1290(6)	1784.3(3)
98	12.1227(6)	1781.6(3)	271	12.1286(7)	1784.2(3)
107	12.1212(7)	1780.9(3)	281	12.1268(7)	1783.4(3)
117	12.1232(6)	1781.8(3)	290	12.1281(7)	1783.9(3)
126	12.1229(8)	1781.7(4)	300	12.1277(6)	1783.7(3)
136	12.1236(6)	1781.9(3)	310	12.1283(6)	1784.0(3)
146	12.1240(6)	1782.1(3)	319	12.1284(6)	1784.1(3)
155	12.1246(7)	1782.4(3)	329	12.1305(6)	1785.0(2)
165	12.1246(6)	1782.4(3)	348	12.1309(6)	1785.2(3)
175	12.1254(6)	1782.7(2)	367	12.1327(7)	1785.9(3)
184	12.1256(6)	1782.8(3)	387	12.1322(7)	1785.8(3)
194	12.1259(6)	1783.0(3)	435	12.1382(7)	1788.4(3)
203	12.1268(6)	1783.4(3)	483	12.1420(8)	1779.0(2)
213	12.1269(6)	1783.4(3)			

*obtained after cooling

TABLE 6. HIGH-TEMPERATURE UNIT-CELL PARAMETERS AND UNIT-CELL VOLUME FOR S8-A

T (°C)	a (Å)	V (Å³)	T (°C)	a (Å)	V (Å³)
20	12.142(1)	1790.3(4)	223	12.152(2)	1794.7(8)
20*	12.139(1)	1788.8(5)	232	12.153(1)	1794.8(5)
39	12.140(1)	1789.3(5)	242	12.154(1)	1795.3(7)
59	12.143(1)	1790.5(6)	252	12.153(2)	1795.1(7)
68	12.143(1)	1790.6(5)	261	12.156(1)	1796.4(7)
78	12.142(2)	1790.0(9)	271	12.155(2)	1795.6(7)
88	12.142(1)	1790.0(5)	281	12.155(2)	1795.9(8)
98	12.144(1)	1790.8(6)	290	12.156(1)	1796.2(7)
107	12.142(1)	1790.3(6)	300	12.159(1)	1797.7(7)
117	12.141(2)	1789.8(7)	310	12.160(1)	1798.2(7)
126	12.143(1)	1790.3(6)	319	12.158(1)	1797.3(6)
136	12.146(1)	1791.8(4)	329	12.160(1)	1797.9(5)
146	12,141(1)	1789.8(5)	339	12.161(1)	1798.5(6)
155	12.145(1)	1791.3(6)	363	12.163(1)	1799.5(7)
165	12.149(1)	1793.3(5)	387	12.166(1)	1800.6(7)
175	12.142(1)	1790.2(7)	411	12.166(1)	1800.8(5)
184	12.151(1)	1794.1(6)	435	12.167(2)	1801.1(7)
194	12.150(2)	1793.5(8)	459	12.168(1)	1801.7(6)
203	12.150(1)	1793.5(7)	483	12.170(1)	1802.7(6)
213	12.154(1)	1795.4(6)			

*obtained after cooling

Optical examination

Crystals were cut parallel to $(001)_{cubic}$ and doubly polished to a thickness of ~30 μm for optical examination. Each section was studied using polarized light and a microscope equipped with a Linkam Scientific Instruments heating stage (model TH1500). The heating stage was calibrated against known phase-transitions and melting points, and is accurate to within ±2°C. The purpose of the optical examination was to determine the temperature of the cubic-to-orthorhombic and orthorhombic-to-rhombohedral phase transitions (Table 3). This was easily accomplished owing to the large changes in the birefringence at each transition. It is possible that a monoclinic phase is stable over a narrow interval of temperature between the rhombohedral and orthorhombic phases, on the basis of studies of end-member $Fe_3B_7O_{13}Cl$ (Schmid & Tippmann 1978). The optical properties of the monoclinic and orthorhombic phases are very similar (and very different from those of the rhombohedral phase) in the $(001)_{cubic}$ section (Schmid & Tippmann 1978). We saw no evidence for the monoclinic phase in the intermediate-composition samples studied here.

Considerable chemical zoning occurs within some of the crystals (Table 2); in such cases, a range of transition temperatures was observed for a given crystal; the temperature of the onset and completion of the phase transition was noted, and the temperature uncertainties reported in Table 3 span the entire range of temperature over which the transition occurred.

Detailed studies of the spontaneous birefringence as a function of temperature were not attempted because the natural crystals contain multiple domains, and detailed measurements on crystals with poor control of multiple domains have been shown to be prone to serious errors (Schmid & Tippmann 1978).

Phase Relations

The phase transitions have previously been documented for synthetically prepared $Mg_3B_7O_{13}Cl$ and $Fe_3B_7O_{13}Cl$ (Schmid & Tippmann 1978). The principal purpose of the current study is to elucidate the phase relations in natural specimens that depart significantly from ideal end-member compositions. Our X-ray powder-diffraction studies at room temperature have suggested the space groups of specimens with intermediate compositions (Table 3), and high-temperature optical examination has permitted the identification of the phase-transition temperature for these specimens (Table 3). The phase relations in the system boracite – trembathite – congolite inferred from our results are given in Figure 2.

All specimens studied undergo a phase transition to the structure of cubic boracite at high temperature (Fig. 2). Upon cooling, specimens of all compositions undergo an apparently first-order transition from the cubic structure to an orthorhombic structure. Specimens rich in Fe undergo an additional first-order transition to the rhombohedral structure prior to reaching room temperature (Fig. 2).

The phase boundary between the stability fields of the cubic and orthorhombic structure is linear in composition–temperature space (Fig. 2), with a slope of 7.1°C per 10 mol.% $Fe_3B_7O_{13}Cl$. The boundary between phases with orthorhombic and rhombohedral

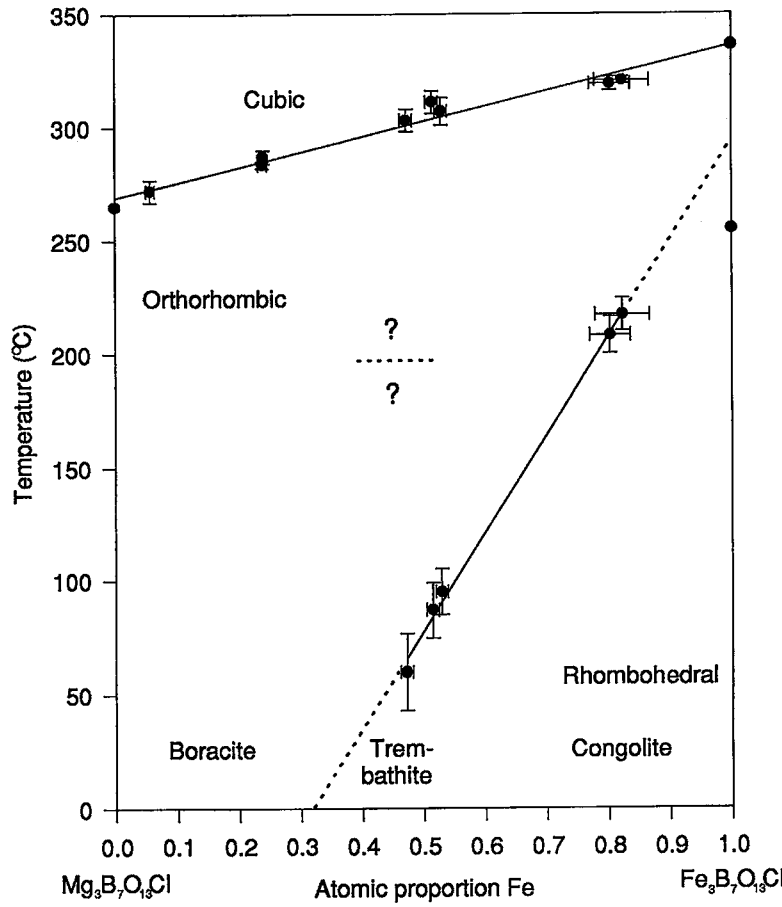

FIG. 2. Phase relations in the series boracite – trembathite – congolite.

symmetry, also linear for the data collected in the present study, is much steeper, with a slope of ~45°C per 10 mol.% $Fe_3B_7O_{13}Cl$. The transition point for the pure Fe end-member (from Schmid & Tippmann 1978) falls below the temperature extrapolated from intermediate compositions, but this behavior is consistent with a plateau effect, as described for other systems by Salje (1995). The extrapolation to more Mg-rich compositions indicates a phase-transition temperature of 25°C for 36 mol.% $Fe_3B_7O_{13}Cl$, corresponding to the formula $(Mg_{1.92}Fe_{1.08})B_7O_{13}Cl$. Thus, at 25°C, boracite is the stable phase over the range $Mg_3B_7O_{13}Cl$ to $(Mg_{1.92}Fe_{1.08})B_7O_{13}Cl$, and the rhombohedral structure is stable from $(Mg_{1.92}Fe_{1.08})B_7O_{13}Cl$ to $Fe_3B_7O_{13}Cl$. At room temperature, specimens with compositions in the range $(Mg_{1.92}Fe_{1.08})B_7O_{13}Cl$ to $(Mg_{1.50}Fe_{1.50})B_7O_{13}Cl$ are trembathite, and those with compositions between $(Mg_{1.50}Fe_{1.50})B_7O_{13}Cl$ and $Fe_3B_7O_{13}Cl$ are congolite. Note that ericaite, defined as the orthorhombic form of $(Fe,Mg)_3B_7O_{13}Cl$ (Kühn & Schaacke 1955), does not occur at room temperature.

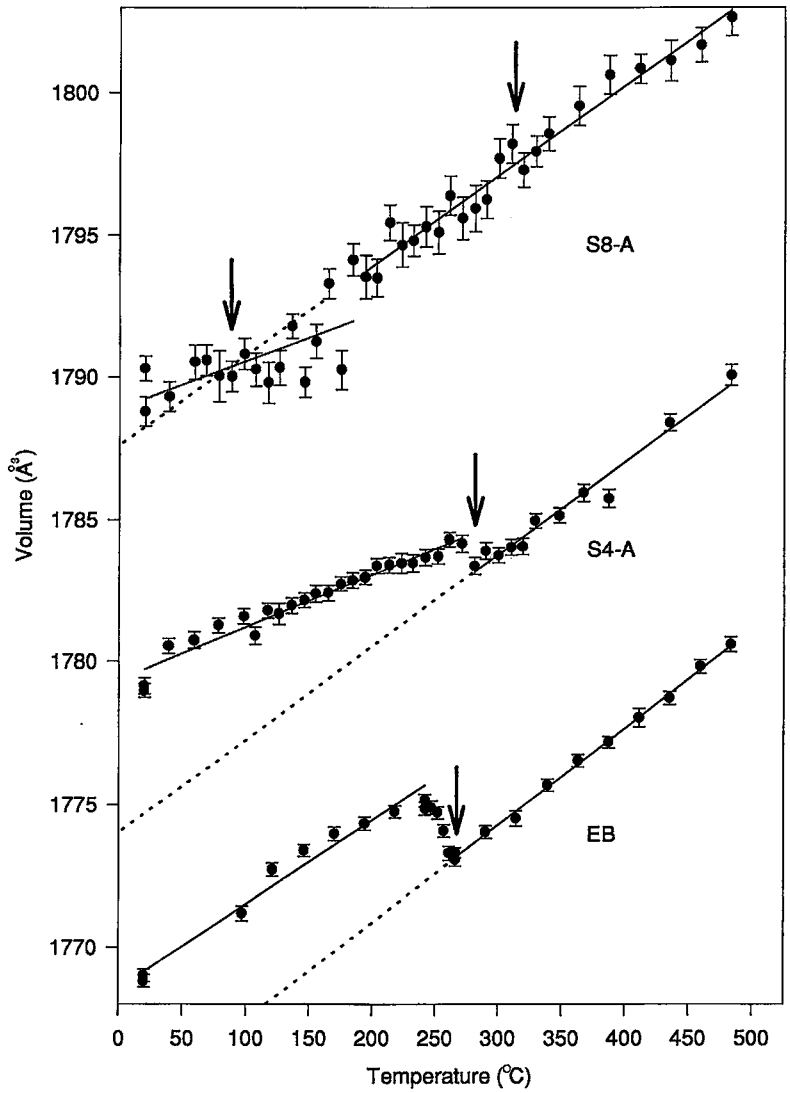

FIG. 3. Unit-cell volume of samples EB $[(Mg_{2.83}Fe_{0.17})B_7O_{13}Cl$, bottom], S4–A $[(Mg_{2.24}Fe_{0.70}Mn_{0.05})B_7O_{13}Cl$, middle] and S8–A $[(Fe_{1.55}Mg_{1.45})B_7O_{13}Cl$, top].

High-Temperature X-Ray Diffraction

Variation of unit-cell volume with temperature

The variation of unit-cell volume with temperature of samples EB, S4–A and S8–A is shown in Figure 3. In each case, the temperature of the phase transition, as determined by optical examination, is indicated by arrows.

Sample EB: The unit-cell volume of sample EB, with composition $(Mg_{2.83}Fe_{0.17})B_7O_{13}Cl$, shows a significant discontinuity at the transition from the cubic to orthorhombic structures. The transition involves an increase in volume of ~0.12% at the transition point (Fig. 3). This transition has been shown to be of first order (Schmid & Tippmann 1978).

Sample S4–A: The unit-cell volume of sample S4–A, with composition $(Mg_{2.24}Fe_{0.71}Mn_{0.06})B_7O_{13}Cl$, shows a discontinuity at the phase transition from the cubic to orthorhombic structures (Fig. 3). In this material, the volume increase at the transition point is ~0.06%.

Sample S8–A: The unit-cell volume of sample S8–A, with composition $(Mg_{1.45}Fe_{1.55})B_7O_{13}Cl$, does not show a significant discontinuity at either of the phase transitions that were detected using optical examination. Owing to the poor peak-to-background ratio, which is due to Fe fluorescence, the unit-cell volumes could not be precisely determined. It is possible that there are discontinuities in the volume at these phase transitions, and that the volume strain is less than the precision of the measurements. The unit-cell volume does show an apparent discontinuity with a volume decrease at ~200°C. A phase transition at this temperature has not been observed using optical examination, but an infrared spectroscopic study does indicate a phase transition near this temperature in the same sample (Burns & Carpenter 1996).

The change of volume at the phase transition in going from the cubic to the orthorhombic structure involves only a relatively small discontinuity (Fig. 3). Notably, the volume discontinuity is largest in the specimen that contains the most Mg; incorporation of Fe in the structure results in a significant decrease in the magnitude of the discontinuity in the volume at the transition.

Volume strain due to the phase transition

The volume strain due to the phase transition is defined as

$$V_S = \frac{V - V_O}{V_O} \qquad (1)$$

where V is the measured unit-cell volume at a given temperature, and V_O is the unit-cell volume extrapolated to the same temperature from the data for the high-temperature phase. The variation of V_S for samples EB and S4–A is shown in Figure 4.

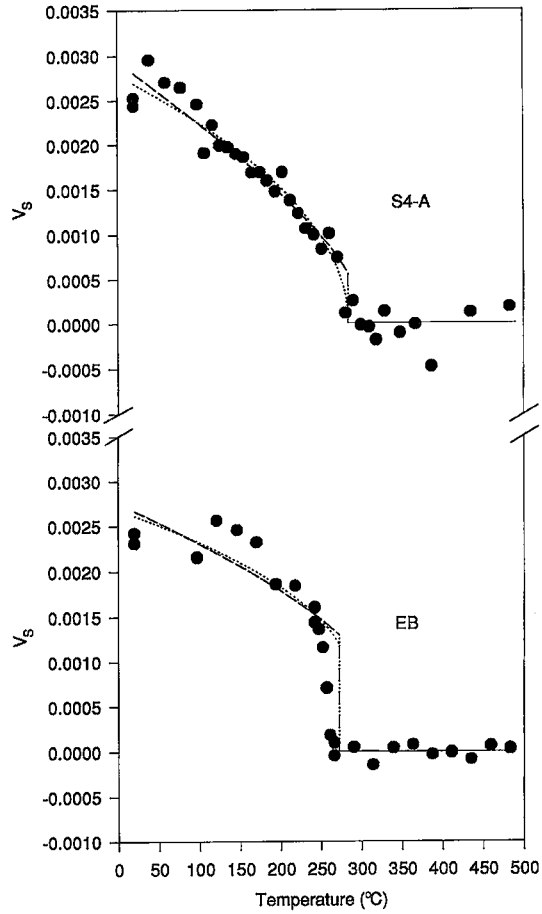

FIG. 4. Volume strain of samples EB [$(Mg_{2.83}Fe_{0.17})B_7O_{13}Cl$, bottom] and S4–A [$(Mg_{2.24}Fe_{0.70}Mn_{0.05})B_7O_{13}Cl$, top]. Broken lines and dotted lines represent the best fit of the 234 (Equation 4) and 246 (Equation 7) potentials, respectively. Data collected for temperatures greater than 252°C were not included in the least-squares fit in the case of sample EB.

V_S is related to the driving order-parameter, Q, for a transition by $V_S \propto Q^2$ in lowest order (*e.g.*, Carpenter 1992). The experimental data thus provide a preliminary means of characterizing the equilibrium evolution of Q through the cubic to orthorhombic transition. For a symmetry change $F\bar{4}3c \leftrightarrow Pca2_1$, including a unit-cell doubling, odd terms are permitted in the Landau expansion for excess free energy (Dvořák & Petzelt

1971, Stokes & Hatch 1988). The general form of this potential (without considering the multicomponent nature of Q) will be that of the standard 234 potential:

$$G = \tfrac{1}{2}a(T - T_C)Q^2 + \tfrac{1}{3}uQ^3 + \tfrac{1}{4}bQ^4 \quad (2)$$

for which the solution for Q (after Bruce & Cowley 1981) is:

$$Q = \tfrac{3}{4}Q_O\{1 + [1 - \tfrac{8}{9}(\frac{T - T_C}{T_{tr} - T_C})]^{1/2}\} \quad (3)$$

The transition must be first order for non-zero values of u and occurs at an equilibrium transition temperature of T_{tr}. At $T = T_{tr}$ the discontinuity in Q is from $Q = 0$ to $Q = Q_O$. Substituting V_S for Q^2 (with the constant of proportionality appearing on both sides of the equation and cancelling out) gives:

$$(V_S)^{1/2} = \tfrac{3}{4}(V_{S,O})^{1/2}\{1 + [1 - \tfrac{8}{9}(\frac{T - T_C}{T_{tr} - T_C})]^{1/2}\} \quad (4)$$

$V_{S,O}$ defines the magnitude of the discontinuity in V_S at T_{tr}. Taking the experimental values of T_{tr} and V_S, a least-squares fitting procedure was used to find values for $V_{S,O}$ and T_C. The best fits for S4–A and EB are shown in Figure 4. A measure of the degree of first-order character is provided by the values $(T_{tr} - T_C)$ and $V_{S,O}$: 60 K, 0.0006 for S4–A ($\sim Mg_{2.24}Fe_{0.71}Mn_{0.06}$) and 313 K, 0.0013 for EB ($\sim Mg_{2.83}Fe_{0.17}$). This implies a trend of decreasing first-order character with increasing substitution of Fe for Mg.

If the value of u in Equation 2 is small, marked first-order character can arise as a consequence of a negative fourth-order coefficient (as occurs in langbeinite: Devarajan & Salje 1984). The appropriate Landau potential has the 246 form:

$$G = \tfrac{1}{2}a(T - T_C)Q^2 + \tfrac{1}{4}bQ^4 + \tfrac{1}{6}cQ^6 \quad (5)$$

with the well-known solution for Q:

$$Q^2 = \tfrac{2}{3}Q_o^2\{1 + [1 - \tfrac{3}{4}(\frac{T - T_C}{T_{tr} - T_C})]^{1/2} \quad (6)$$

Substituting V_S for Q^2 gives:

$$V_S = \tfrac{2}{3}V_{S,O}\{1 + [1 - \tfrac{3}{4}(\frac{T - T_C}{T_{tr} - T_C})]^{1/2}\} \quad (7),$$

which has been used to find values for T_C and $V_{S,O}$, as before. The fits are shown for comparison in Figure 4, and the values obtained for $(T_{tr} - T_C)$, $V_{S,O}$ are: $\sim$0.01 K, 1.6×10^{-5} for S4–A, and 39 K, 0.0012 for EB. The trend of decreasing first-order character with increasing iron is again evident, though the fit parameters imply that the transition is closer to being continuous. The transition in S4–A would be close to being tricritical ($Q^4 \propto T$, $V \propto T$) in this interpretation.

The data clearly are insufficiently precise to allow any conclusive distinction between the two general forms of governing potential at this stage. It is interesting to note, however, that the trend toward tricritical or second-order character with increasing Fe content coincides with a decrease in the absolute values of the volume strains in the three samples for which cell-parameter data were obtained. Coupling between Q and V_S causes renormalization of the fourth-order coefficient, b, and increasing V_S is well known to promote a tendency to first-order character for a transition (*e.g.*, Bruce & Cowley 1981). If the correct potential for the transition is eventually shown to have the 246 form, the change in volume strain with composition may be significant in causing the changing thermodynamic character. This view of the transition is not entirely consistent with the evidence from birefringence measurements, which show that the cubic to orthorhombic transition in boracite is almost invariably first order in character (this study; Schmid & Tippmann 1978).

Symmetry-breaking strain due to the phase transition

Within the resolution of the X-ray-diffraction experiments, the unit-cell parameters of the orthorhombic and rhombohedral phases remain dimensionally cubic below the transition. Despite using monochromated Cu$K\alpha_1$ X-radiation and a focusing diffraction-geometry, no peak splitting is observed, and attempts to refine the unit-cell parameters with orthorhombic or rhombohedral constraints consistently gives a cubic unit-cell within error. The symmetry-breaking strain is thus very small. To investigate this further, a single Voigt peak was fit to the diffraction peak corresponding to the $(400)_{orthorhombic}$, $(040)_{orthorhombic}$ and $(224)_{orthorhombic}$ reflections that occur at the same position if the structure is cubic. However, if the structure is orthorhombic or rhombohedral, these reflections need not occur at exactly the same location. Generally, the full-width at half-maximum (FWHM) for a given diffraction-peak will gradually increase with temperature as a result of thermal diffuse scattering. However, the dependence of peak width on temperature may be dominated by the phase transitions.

The variation of the peak FWHM with temperature for samples EB, S4–A and S8–A is shown in Figure 5. For sample EB, the FWHM remains essentially constant at $\sim$0.117°2θ in the cubic phase, but the FWHM steadily increases with decreasing temperature below the phase transition. The same behavior is exhibited by the FWHM for the corresponding peak in the diffractograms of samples S4–A and S8–A. This increase in the peak FWHM probably results

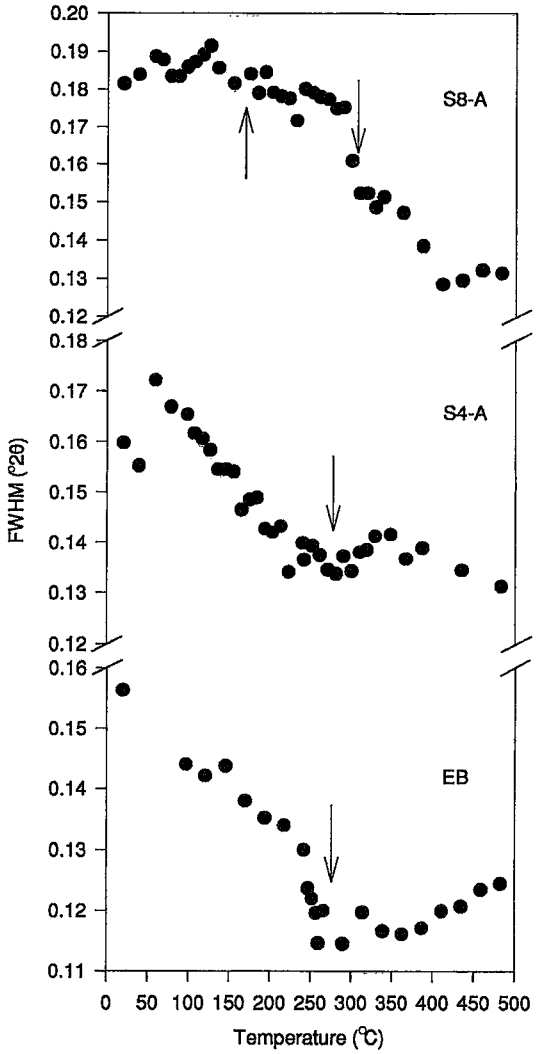

FIG. 5. Peak full-width at half-maximum (FWHM) for the peak corresponding to the overlapping $(400)_{orthorhombic}$, $(040)_{orthorhombic}$ and $(224)_{orthorhombic}$ reflections in the diffractograms of sample EB [$(Mg_{2.83}Fe_{0.17})B_7O_{13}Cl$, bottom], S4–A [$(Mg_{2.24}Fe_{0.70}Mn_{0.05})B_7O_{13}Cl$, middle] and S8–A [$(Fe_{1.55}Mg_{1.45})B_7O_{13}Cl$, top].

because the unit cells of the low-symmetry phases do not remain exactly dimensionally cubic. Thus, although the symmetry-breaking strain due to the phase transition is small in these phases, it is readily observable by examining the FWHM of selected diffraction-peaks.

DISCUSSION

The borate deposits at Sussex, New Brunswick, contain the three boracite-group minerals boracite, trembathite and congolite. The range of chemical compositions displayed by the boracite-group minerals (both bulk crystal and zoning within the same crystal) suggests that a complete solid-solution series from $Mg_3B_7O_{13}Cl$ to $Fe_3B_7O_{13}Cl$ may occur. This study has also revealed the phase relations in this series.

Any boracite-group mineral that crystallizes in the stability field of the cubic phase will undergo a structural transition, or transitions, upon cooling. These structural transitions will induce microstructures in the crystals, explaining why most natural and synthetic crystals of boracite-group minerals contain multiple domains and complex lamellar configurations (Schmid & Tippmann 1978) and display anomalous optical properties. However, a crystal that grew at a temperature below the cubic-to-orthorhombic transition in the case of Mg-rich compositions, or the orthorhombic-to-rhombohedral transition if the crystal is Fe-rich, will not have undergone a phase transition upon cooling. Such a crystal will not contain transformation-induced microstructures. Thus, the thermal history of the borate deposit is recorded by the presence or absence of transformation-induced microstructures in the boracite-group minerals. The presence of transformation-induced microstructures in these crystals provides a minimum temperature of crystallization, whereas an absence of transformation-induced microstructures places an upper bound on the temperature of crystallization.

Heide *et al.* (1980) discussed the occurrence of a rhombic form of boracite, which they referred to as "stassfurtite" in the Zechstein deposits of Germany. This phase has never been accepted as a valid mineral species. Examination of Figure 2 indicates that the rhombohedral structure will only be stable at 25°C if the structure contains at least 36 mol.% $Fe_3B_7O_{13}Cl$, whereas "stassfurtite" reportedly is pure $Mg_3B_7O_{13}Cl$. Heide *et al.* (1980) provided DTA curves for four specimens, including one of "stassfurtite". The DTA curve for this specimen reveals only one absorption event, which occurs at ~265°C, exactly where the cubic-to-orthorhombic phase transition occurs in $Mg_3B_7O_{13}Cl$. Thus, in light of this study, it seems very unlikely that "stassfurtite" is anything other than boracite. Heide *et al.* (1980) also reported a DTA curve for an Fe-rich specimen. The results indicate that more than one phase transition occurs on heating. The first transition (or possibly transitions) occurs at ~215°C, whereas the other occurs at ~320°C, values in good agreement with the phase diagram reported here in Figure 2.

In order for boracite-type phases to be used in applications that take advantage of their ferroelectric and ferroelastic properties, a composition having a

very small shear angle is required to prevent cracking. Although Schmid & Tippmann (1978) have suggested that solid-solution series between certain boracite-type phase end-members may exhibit small amounts of structural strain, to the best of our knowledge, this is the first study of the phase transitions in any boracite-type phase of an intermediate composition. In the current study of the series $Mg_3B_7O_{13}Cl$ – $Fe_3B_7O_{13}Cl$, both the character of the phase transitions and the structural strains due to the phase transitions are significantly dependent upon the composition of the specimen. Our results indicate that the structural strain associated with the cubic-to-orthorhombic transition decreases significantly with increasing Fe content in the series $Mg_3B_7O_{13}Cl$ – $Fe_3B_7O_{13}Cl$. Thus, it may be possible to attain a desired behavior by altering the composition of the boracite phase by substitution at the metal site(s).

Acknowledgements

This work was supported by the Natural Sciences and Engineering Research Council of Canada in the form of a Post-Doctoral Fellowship to PCB. Clare Hall, Cambridge, supported PCB with a Research Fellowship. We thank Drs. Gordon J. Nord, Jr. and Peter J. Heaney for their thoughtful reviews of the manuscript and Robert F. Martin for editorial work that improved the clarity of this contribution.

References

Appleman, D.E. & Evans, H.T., Jr. (1973): Job 9214: indexing and least-squares refinement of powder diffraction data. *U.S. Geol. Surv., Comput. Contrib.* **20** (*NTIS Doc.* **PB2-16188**).

Bruce, A.D. & Cowley, R.A. (1981): *Structural Phase Transitions.* Taylor and Francis, London, U.K.

Burns, P.C. (1995): X-ray powder diffraction data for the identification of boracite-group minerals. *Powder Diff.* **10**, 250-260.

_____ & Carpenter, M.A. (1996): Phase transitions in the series boracite – trembathite – congolite: an infrared spectroscopic study. *Can. Mineral.* **34** (in press).

_____, Grice, J.D. & Hawthorne, F.C. (1995): Borate minerals. I. Polyhedral clusters and fundamental building blocks. *Can. Mineral.* **33**, 1131-1151.

_____, Hawthorne, F.C. & Stirling, J.A.R. (1992): Trembathite, $(Mg,Fe)_3B_7O_{13}Cl$, a new borate mineral from the Salt Springs potash deposit, Sussex, New Brunswick. *Can. Mineral.* **30**, 445-448.

Carpenter, M.A. (1992): Thermodynamics of phase transitions in minerals: a macroscopic approach. *In* The Stability of Minerals (G.D. Price & N.L. Ross, eds.). Chapman & Hall, London, U.K. (172-215).

Devarajan, V. & Salje, E. (1984): Phase transitions in $K_2Cd_2(SO_4)_3$: investigation of the non-linear dependence of spontaneous strain and morphic birefringence on order parameter as determined from excess entropy measurements. *J. Phys. C* **17**, 5525-5537.

Dowty, E. & Clark, J.R. (1973): Crystal-structure refinements for orthorhombic boracite, $Mg_3ClB_7O_{13}$, and a trigonal, iron-rich analogue. *Z. Kristallogr.* **138**, 64-99.

Dvořák, V. & Petzelt, J. (1971): Symmetry aspect of the phase transitions in boracites. *Czech. J. Phys.* **B21**, 1141-1152.

Grice, J.D., Burns, P.C. & Hawthorne, F.C. (1994): Determination of the megastructures of the borate polymorphs pringleite and ruitenbergite. *Can. Mineral.* **32**, 1-14.

Heide, K., Franke, H. & Brückner, H.-P. (1980): Vorkommen und Eigenschaften von Boracit in den Zechsteinsalzlagerstätten der DDR. *Chem. Erde* **39**, 201-232.

_____ & Völksch, G. (1979): Rasterelektronenmikroskopische Untersuchungen zur Morphologie von Boracit, Ascharit und Sulfoborit aus den Zechsteinlagerstätten der DDR. *Chem. Erde* **38**, 223-232.

Honea, R.M. & Beck, F.R. (1962): Chambersite, a new mineral. *Am. Mineral.* **47**, 665-671.

Ito, T., Morimoto, N. & Sadanaga, R. (1951): The crystal structure of boracite. *Acta Crystallogr.* **4**, 310-316.

Kühn, R. & Schaacke, I. (1955): Vorkommen und analyse der Boracit- und Ericaitkristalle aus dem Salzhorst von Wathlingen-Hänigsen. *Kali und Steinsalz* **11**, 33-42.

Mandarino, J.A., Rachlin, A.L., Dunn, P.J., Le Page, Y., Back, M.E., Murowchick, B.L., Ramik, R.A. & Falls, R.B. (1990): Redefinition of volkovskite and its description from Sussex, New Brunswick. *Can. Mineral.* **28**, 351-356.

Mendoza-Alvarez, M.-E., Yvon, K., Depmeier, W. & Schmid, H. (1985): Structure refinement of trigonal iron–chlorine boracite. *Acta Crystallogr.* **C41**, 1551-1552.

Nelmes, R.J. (1974): Structural studies of boracites. A review of the properties of boracites. *J. Phys. C: Solid State Phys.* **7**, 3840-3854.

Rachlin, A.L., Mandarino, J.A., Murowchick, B.L., Ramik, R.A., Dunn, P.J. & Back, M.E. (1986): Mineralogy of hilgardite-4*M* from evaporites in New Brunswick. *Can. Mineral.* **24**, 689-693.

Roberts, A.C., Stirling, J.A.R., Grice, J.D., Burns, P.C., Roulston, B.V., Curtis, J.D. & Jambor, J.L. (1993): Pringleite and ruitenbergite, polymorphs of $Ca_9B_{26}O_{34}(OH)_{24}Cl_4{\cdot}13H_2O$, two new mineral species from Sussex, New Brunswick. *Can. Mineral.* **31**, 795-800.

ROULSTON, B.V. & WAUGH, D.C.E. (1981): A borate mineral assemblage from the Penobsquis and Salt Springs evaporite deposits of southern New Brunswick. *Can. Mineral.* **19**, 291-301.

_____ & _____ (1983): Stratigraphic comparison of the Mississippian potash deposits in New Brunswick, Canada. *Sixth International Symposium on Salt* **1**, 115-127.

SALJE, E.K.H. (1995): Chemical mixing and structural phase transitions: the plateau effect and oscillatory zoning near surfaces and interfaces. *Eur. J. Mineral.* **7**, 791-806.

_____, GRAEME-BARBER, A., CARPENTER, M.A. & BISMAYER, U. (1993): Lattice parameters, spontaneous strain and phase transitions in $Pb_3(PO_4)_2$. *Acta Crystallogr.* **B49**, 387-392.

SCHMID, H. (1970): Trigonal boracites – a new type of ferroelectric and ferromagnetoelectric that allows no 180° electric polarization reversal. *Phys. Stat. Sol.* **37**, 209-223.

_____ & TIPPMANN, H. (1978): Spontaneous birefringence in boracites – measurements and applications. *Ferroelectrics* **20**, 21-36.

STOKES, D.M. & HATCH, H.T. (1988): *Isotropy Subgroups of the 230 Crystallographic Space Groups.* World Scientific, London, U.K.

SUENO, S., CLARK, J.R., PAPIKE, J.J. & KONNERT, J.A. (1973): Crystal-structure refinement of cubic boracite. *Am. Mineral.* **58**, 691-697.

WENDLING, E., HODENBERG, R.V. & KÜHN, R. (1972): Congolit, der trigonale Eisenboracit. *Kali und Steinsalz* **6**, 1-3.

Received October 7, 1995, revised manuscript accepted March 13, 1996.